Direct Observation of Smectic Layers in Thermotropic Liquid Crystals

C. Zhang,[1] M. Gao,[2] N. Diorio,[1] W. Weissflog,[3] U. Baumeister,[3] S. Sprunt,[4] J. T. Gleeson,[4] and A. Jákli[1,2,*]

[1]*Chemical Physics Interdisciplinary Program, Kent State University, Kent, Ohio 44242, USA*
[2]*Liquid Crystal Institute, Kent State University, Kent, Ohio 44242, USA*
[3]*Department of Chemistry and Physical Chemistry, Martin Luther University Halle-Wittenberg,*
von-Danckelmann-Platz 4, 06120 Halle, Germany
[4]*Department of Physics, Kent State University, Kent, Ohio 44242, USA*
(Received 22 May 2012; published 7 September 2012)

We demonstrate subnanometer resolution cryo-TEM imaging of smectic layers in the smectic and nematic phases of two bent-core liquid crystals. Our results show perfect periodicity over several hundred layers in the smectic phase and also provide the first direct evidence of smectic clusters on length scales of 30–50 nm in a nematic liquid crystal. The results are corroborated with small angle x-ray scattering measurements. The observation of smectic clusters in the nematic phase is of special interest in bent-core liquid crystals, where the smectic clusters are stable over wide temperature ranges, in contrast to the well-known pretransitional "cybotactic" clusters that appear only in the vicinity of a bulk smectic phase. The means to characterize and manipulate this nanoscale molecular order could open up completely new liquid crystal-based technologies.

Cryo-transmission electron microscopy (cryo-TEM) is a well developed technique to study nanostructures of biological materials and lyotropic liquid crystals [1–6]. Nanostructures of thermotropic liquid crystals are usually studied by freeze-fracture TEM, where the surface of a fractured cryo-fixed sample is coated by layers of a heavy metal and carbon, and the resulting replica film is imaged [7,8]. This method can provide a resolution of about 2 nm allowing for the observation of defects [9–11], nanofilaments [12,13], and twist grain boundaries [14,15]. Individual layers can be barely resolved by freeze-fracture TEM [15] and require optical diffraction [14] or additional atomic force microscopy [16]. Cryo-TEM directly images soft materials, whose structure is fixed by quenching to cryogenic temperatures. A beam of electrons is transmitted through a thin specimen layer (typically less than 100 nm thick), and then the transmitted beam is expanded (which gives magnification) and focused onto an imaging device [17]. To achieve good contrast, one typically needs two or more component compounds having different electron densities; that is why biological objects and lyotropic liquid crystals are good candidates for cryo-TEM studies.

Single component thermotropic liquid crystal (LC) compounds have applications ranging from flat panel displays to biological sensors, and understanding their nanoscale structure is extremely important for possible future applications. Traditionally, the most important structural probe of LC order has been x-ray scattering, particularly at small angles (SAXS). However, SAXS cannot directly reveal full details of the spatial distribution of ordered structures, and the interpretation of short-range order—e.g., local smecticlike packing of molecules in a nematic (purely orientationally ordered) phase—can be difficult. For these reasons, a direct

nanoscopic imaging of different liquid crystalline mesophases is particularly valuable. TEM imaging of thermotropic liquid crystals is challenging for several reasons. They are composed of low molecular weight organic molecules only, and there is a relatively weak contrast between the rigid, more electron dense, aromatic cores and the flexible, less electron dense, hydrocarbon tails. Moreover, in order for this contrast not to be averaged out as the electron beam passes through the sample, the molecules must be positionally ordered into layers, which in turn must be almost completely perpendicular to the beam. Specifically, the deviation from perpendicular must be less than $\alpha < \tan^{-1}(d/L)$, where $d \sim 3$ nm is the layer periodicity and $L < 100$ nm is the specimen's thickness. For uniform tilt along the thickness, this means less than 2° of tilt. It also implies that periodicity measured from a high contrast image of the layers differs from the actual periodicity by less than 0.1%.

Here we demonstrate cryo-TEM imaging of smectic layers with subnanometer resolution. Our results reveal perfect periodicity over several hundred layers in the smectic phase and also show the first direct evidence of smectic clusters on length scales of 30–50 nm in a nematic liquid crystal. This latter observation is of special interest in bent-core liquid crystals [18], where the smectic clusters are stable over wide temperature ranges [19], in contrast to the well-known pretransitional "cybotactic" clusters [20] that appear only in the vicinity of a bulk smectic phase.

Studies were conducted on two bent-core (BC) materials: bis(4-*n*-octanoyloxyphenyl) 2-methylisophthalate and bis(4-*n*-decanoylphenyl) 2-methylisophthalates. The molecular structures and phase sequences of both materials are shown in Figs. 1(a) and 1(b), respectively. The compounds differ in the length of the terminal chains and their

(a)
3RBC-S
Iso 118.6 SmA 66.5 Cr

(b)
3RBC-N
Iso 100.1 N 62.5 Cr

(c)
Continuous carbon film
Liquid crystal
Copper grid
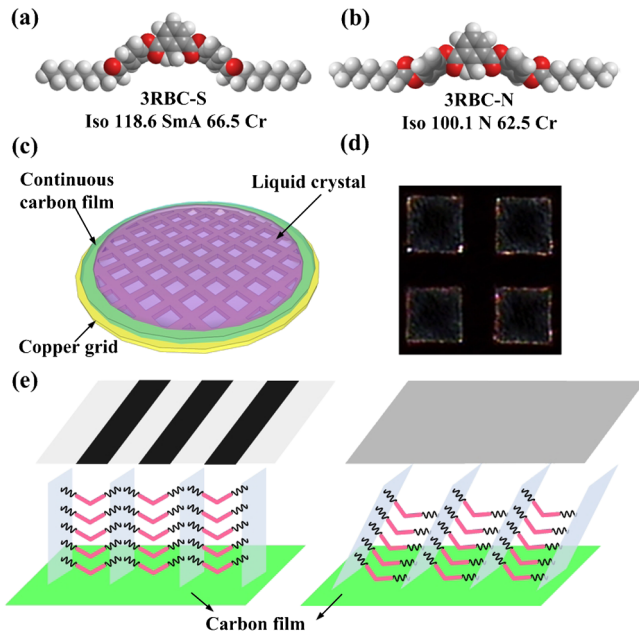
(d)

(e)
Carbon film

FIG. 1 (color online). Summary of sample preparation and TEM experimental conditions. (a),(b) Molecular structure, code, and phase sequence on heating and cooling of the compounds 3RBC-S and 3RBC-N, respectively. (Cr, N, SmA, and Iso denote crystal, nematic, smectic-A, and isotropic liquid phases, respectively; numbers are transition temperatures in °C). (c) Illustration of the LC films deposited on TEM grids coated with a carbon film. (d) Polarizing optical microscopy texture of a 100 nm thick LC film. The gray image indicates planar alignment (average molecular long axis parallel to the substrates). (e) Illustration of the TEM imaging when the layers are perpendicular to the substrates (left) and when they are tilted by more than a few degrees (right).

connection to the outer phenyl rings. The longer compound with a carbonyl connecting group [Fig. 1(a)] has a smectic-A mesophase, whereas the shorter compound has a carboxylic linking group [Fig. 1(b)] and exhibits a nematic mesophase. For these reasons we shall refer to them as 3RBC-S and 3RBC-N, respectively. The stretched molecular length (as determined by ChemDraw) of 3RBC-S is 3.99 nm, while that of 3RBC-N is 3.76 nm. The chemical synthesis, purification, and characterization of the basic properties of the two compounds are described elsewhere [21].

To achieve planar molecular alignment (and smectic layers normal to the substrate), the LC samples were dissolved in chloroform, and the solution was dispersed on a TEM grid coated with plasma treated, continuous, carbon film [Fig. 1(c)]. The chloroform was then evaporated away. Because of the hydrophilic nature of the carbon film, the molecular core prefers to be in contact with the substrate, and the aliphatic tails avoid the film and point slightly out [Fig. 1(d)]. This arrangement is also facilitated by the molecules' bent shape. The thickness of the liquid crystal film could be set to be between 50 and 100 nm by adjusting the volume of the solution and the concentration of the
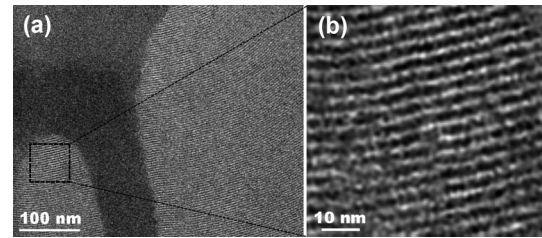

FIG. 2. A typical cryo-TEM image of 3RBC-S quenched from 87 °C. (a) A 350 nm $\times$ 500 nm area of the sample. Dark domains correspond to thick areas, and the periodic stripe texture corresponds to a less than 100 nm thick area with smectic layers perpendicular to the substrate. (b) Enlarged image of the 70 nm $\times$ 70 nm area enclosed by the rectangle in (a), illustrating the details of the layer structure. Dark stripes correspond to the aromatic cores and lighter areas to the hydrocarbon tails.

chloroform. Films in this thickness range appeared pale gray in transmission polarizing microscopy [see Fig. 1(d)] indicating uniform planar alignment over micrometer ranges. The LC films were heated to the isotropic phase, cooled to the desired temperatures, and then rapidly (within less than a second at room temperature) quenched in liquid nitrogen (-196 °C) to preserve the liquid crystalline structures. Details of sample preparation are described in Supplemental Material [22].

Cryo-TEM measurements were performed in a FEI Tecnai F20 microscope, operating at 200 kV and equipped with a Schottky field emission gun and a twin-blade anti-contaminator. The microscope provides 0.24 nm point-to-point resolutions and a 0.15 nm information limit in TEM mode. The image resolution, as determined from the 25%–75% edge resolution test performed across a periodic structure, is found to be better than 0.7 nm (see Supplemental Material [22]). As liquid crystal films are sensitive to the electron beam irradiation, the films were normally previewed rapidly at a dose of 20 e^-/nm^2. Selected areas were then imaged at a dose level of 200 e^-/nm^2, which we found not to cause radiation damage.

Figure 2 shows a typical TEM image of a 350 nm $\times$ 500 nm area, and a magnified image of a 70 nm $\times$ 70 nm area, in a film of 3RBC-S quenched from the smectic phase at 87 °C after slow cooling of the sample from the isotropic to the smectic phase. The dark regions in the image correspond to thicker domains of the film (from several hundreds of nanometers to microns). In the thinner (approximately 100 nm thick) areas, we clearly observe that the periodic structure is aligned (in a roughly uniform direction) across an area larger than the image size—over 1 μm (or 300 times the layer spacing). This indicates a nucleation of upright layers over at least micron-sized domains. The thick parts of the film do not show periodicity, which probably indicates that the layers tilt significantly near the free surface of the film—i.e., the influence of the planar-aligning carbon surface does not penetrate effectively through the entire film thickness. The enlargement in Fig. 2 shows the details of the
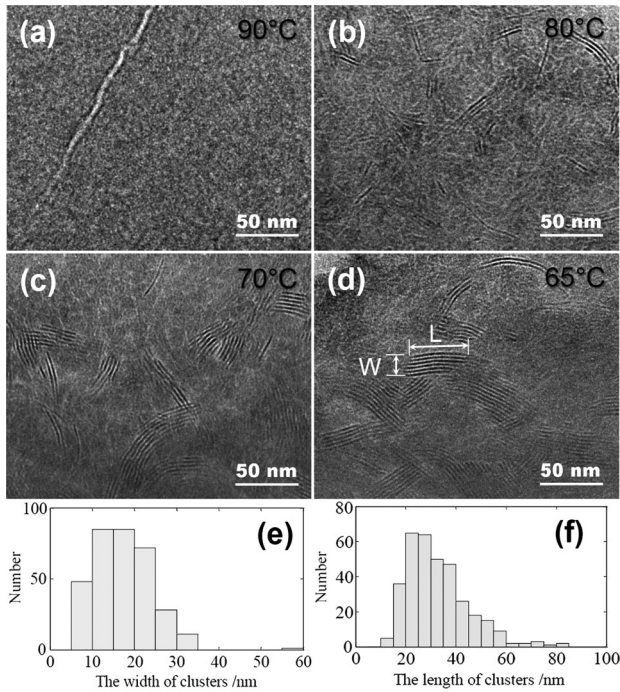
FIG. 3. Summary of the cryo-TEM observations on 3RBC-N. TEM images after quenching from 90 (a), 80 (b), 70 (c), and 65 °C (d). Striped domains are smectic clusters of molecules, which are oriented in different directions even in overlapping spots at different depths in the sample. (e) Histogram of the width of the layered clusters at 70 °C. (f) Histogram of the length of the clusters at 70 °C. The cluster size increases to lower quench temperatures.

well-defined layering with a periodicity of 3.7 nm. Since the contrast reflects electron density, the darker areas correspond to the aromatic rigid core, and the lighter ones represent the region occupied by the less dense, flexible hydrocarbon tails.

Compared to 3RBC-S, the nanostructure of nematic 3RBC-N exhibits only short-range layering that depends on the sample temperature prior to quenching. Figures 3(a)–3(d) show typical images of samples quenched from the nematic phase at 90, 80, 70, and 65 °C, respectively.

At 90 °C [Fig. 3(a)], 3RBC-N shows no distinctive structure except for a few cracks which presumably occurred during quenching. As the prequench temperature decreases, we find large areas with an increasing number of layered domains [Figs. 3(b)–3(d)]. These extend a few tens of nanometers parallel to the layers (length) and contain 3–7 layers. The layer spacing in the domains (or clusters) varies between 3.1 and 3.5 nm and is basically independent of the prequench temperature. Lower prequench temperatures lead to more layers in the ordered domains, and as much as 20% of the areas can be covered by layered domains [see Fig. 3(d)]. The increase of the cluster area at lower quench temperatures indicates that individual clusters must exist for at least the time it takes to freeze the specimen (< 1 ms) in the freezing fluid. In addition to

individual domains, in 70 and 65 °C [Figs. 3(c) and 3(d)] overlapping layered domains are seen too, showing that depth of field exceeds the layer depth in a single cluster. Although the director is uniform over the micrometer range [as polarizing optical microscopy texture in Fig. 1(d) shows], the direction of the layers in separate clusters—even in one spot but at different heights—varies by nearly as much as 90°, which is in sharp contrast with the long-range, uniform layer alignment observed in the sample of 3RBC-S. This is due to the tilt between the director and the layer normal, which we cannot see by cryo-TEM, but the SAXS pattern clearly shows, as we will discuss below.

We statistically analyzed a few hundred individual molecular clusters exhibiting smectic layers. Histograms showing the distribution of the width (w) and length (l) of the clusters after quenching from 70 °C are shown in Figs. 3(e) and 3(f), respectively. The full width at half maximum (FWHM) for the length is 25 ± 2.5 nm, while for the width it is 20 ± 2.5 nm. Interestingly, the shorter clusters show fairly straight layers; however, in the longer ones observed ($l > 3w$), we see bent layers with curvature ~ 0.01 nm^{-1} [see Fig. 3(d)]. This bend is probably due to director fluctuations. For samples with lower prequench temperatures, the FWHM of the distribution decreases.

In order to definitively correlate the origin of the structures described above with smectic layering, we performed SAXS measurements on the same materials at the National Synchrotron Light Source (NSLS, beam line X6B). Details of the experimental conditions are given in Supplemental Material [22], and elsewhere [19]. A summary of the results is shown in Fig. 4.

In 3RBC-S [Fig. 4(a)], we observe a direct isotropic to smectic transition; the two sharp, intense peaks below the transition indicate a smectic A mesophase. Measurements on surface aligned samples also confirmed the SmA structure. The periodicity of the layers is 3.7 nm and barely changes with temperature until crystallization, which is in agreement with the TEM observations. The two-dimensional SAXS pattern for 3RBC-N reveals the expected isotropic diffuse ring pattern above the isotropic-nematic transition. Below the transition to the nematic phase, the ring condenses to two broad arcs centered at $q = 0.19$ Å^{-1} and elongated in the direction normal to the magnetic field used to align the nematic director (average long molecular axis). The peak position in q space corresponds to short-range smectic A-type layering with a layer spacing of $d = 3.31$ nm. This is in excellent agreement with the cryo-TEM results, where a periodicity between 3.1 and 3.5 nm was observed. At lower temperatures, the arcs take on a peanut shape, and each arc splits into two broad peaks, showing the onset of layer tilt (smectic-C-like short-range order). This shows that the wide range of layer directions evident in the TEM image [Fig. 3(d)] is due to layer tilt with respect to the
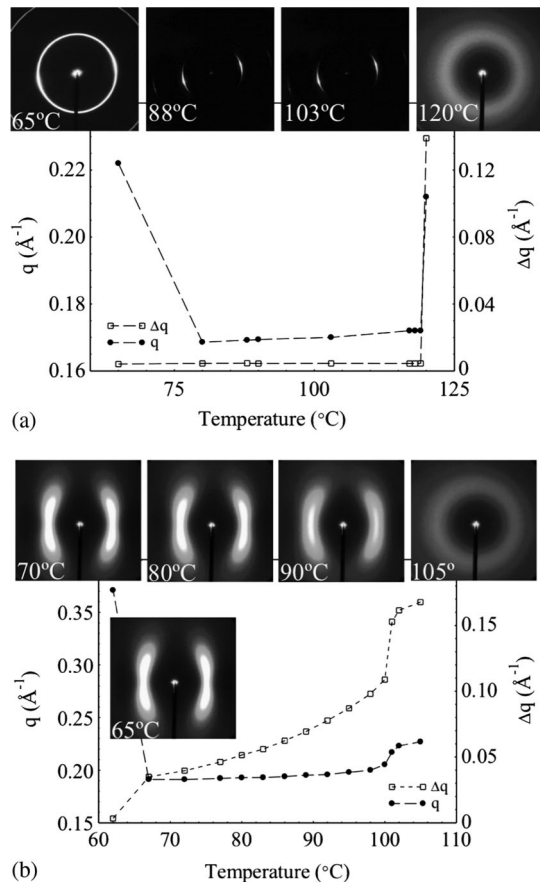
FIG. 4. Summary of the experimental results from SAXS measurements (a) for 3RBC-S and (b) for 3RBC-N. The wave number (q) corresponding to the peak scattered intensity (left vertical axis) and the full width at half maximum (Δq) (right vertical axis) are plotted as a function of temperature for the two compounds. Also shown are 2D diffraction patterns for various temperatures.

molecular orientation. On the right axes of Fig. 4(b), we see that the full width at half maximum (Δq) decreases with temperature from $\Delta q = 0.17$ Å^{-1} in the isotropic phase to $\Delta q = 0.04$ Å^{-1} just above the crystallization temperature. This indicates that on average the width [23] of the smectic domains increases from roughly two to eight molecular lengths, again in agreement with the cryo-TEM results in Fig. 3. Comparison of the normalized integrated SAXS intensities shows a 25-times larger value for 3RBC-S than 3RBC-N. Although we cannot definitively exclude the possibility that the areas between the layered domains are filled with clusters of layers tilted away the 2° vertical alignment window, the much weaker SAXS signal of 3RBC-N suggests that on average only a fraction of its volume is filled with smectic clusters and the majority is in the nematic state. It might happen that, in the areas where we see the clusters by TEM, the majority of them have vertical layers, such as in case of the 3RBC-S material shown in Fig. 2. Overlapping clusters with different layer directions probably have uniform

director structure but with oppositely tilted layers. The variation of the tilt direction is due to the wide distribution of the director tilt seen in Fig. 4(b).

In summary, cryo-TEM on thermotropic liquid crystals proves to be an extremely powerful tool, complementary to SAXS, for detailed analysis on the nanoscale characteristics of thermotropic liquid crystals. In addition to basic structural information, it reveals the shape, distribution, and proportion of nanostructures, details that SAXS cannot provide. These details are important to developing improved means to characterize and manipulate this nanoscale molecular order, which could open up completely new liquid crystal-based technologies.

*Corresponding author.
ajakli@kent.edu

[1] F. P. Booy and A. G. Fowler, Int. J. Biol. Macromol. **7**, 327 (1985).
[2] J. Gustafsson, H. Ljusberg-Wahren, M. Almgren, and K. Larsson, Langmuir **13**, 6964 (1997).
[3] L. Sagalowicz, R. Mezzenga, and M. E. Leser, Curr. Opin. Colloid Interface Sci. **11**, 224 (2006).
[4] P. T. Spicer, K. L. Hayden, M. L. Lynch, A. Ofori-Boateng, and J. L. Burns, Langmuir **17**, 5748 (2001).
[5] J. Gustafsson, H. Ljusberg-Wahren, M. Almgren, and K. Larsson, Langmuir **12**, 4611 (1996).
[6] M. Allain, Europhys. Lett. **2**, 597 (1986).
[7] R. Steere, J. Biophys. Biochem. Cytol. **3**, 45 (1957).
[8] O. Mondain-Monval, Curr. Opin. Colloid Interface Sci. **10**, 250 (2005).
[9] M. J. Costello, S. Meiboom, and M. Sammon, Phys. Rev. **29**, 2957 (1984).
[10] M. Kleman, C. E. Williams, M. J. Costello, and T. Gulik-Krztwicki, Philos. Mag. **35**, 33 (1977).
[11] P. Moreau, L. Navailles, J. Giermanska-Kahn, O. Mondain-Monval, F. Nallet, and D. Roux, Europhys. Lett. **73**, 49 (2006).
[12] D. A. Coleman *et al.*, Science **301**, 1204 (2003).
[13] L. E. Hough *et al.*, Science **325**, 452 (2009).
[14] K. Ihn, J. Zasadzinski, R. Pindak, and A. Slaney, Science **258**, 275 (1992).
[15] J. Fernsler *et al.*, Proc. Natl. Acad. Sci. U.S.A. **102**, 14 191 (2005).
[16] L. E. Hough *et al.*, Science **325**, 456 (2009).

[17] D. B. Williams and C. B. Carter, *Transmission Electron Microscopy: A Textbook for Materials Science* (Plenum, New York, 1996).

[18] H. Takezoe and Y. Takanishi, Jpn. J. Appl. Phys. **45**, 597 (2006).

[19] S. H. Hong, R. Verduzco, J. C. Williams, R. J. Twieg, E. DiMasi, R. Pindak, A. Jákli, J. T. Gleeson, and S. Sprunt, Soft Matter **6**, 4819 (2010).

[20] A. de Vries, Mol. Cryst. Liq. Cryst. **10**, 219 (1970).

[21] W. Weissflog *et al.*, Soft Matter **8**, 2671 (2012).

[22] See Supplemental Material at http://link.aps.org/supplemental/10.1103/PhysRevLett.109.107802 for further information on sample preparation, polarizing optical microscopy, cryo-TEM measurements, and SAXS measurements.

[23] O. Francescangeli, M. Laus, and G. Galli, Phys. Rev. E **55**, 481 (1997).